Climate, Dust, and Fire Across the Eocene-Oligocene Transition, Patagonia

METHODS

Sampling

The Sarmiento Formation is divided into six members, most of which are laterally discontinuous along the main outcrop (Bellosi, 2010b), along the shore of Lake Colhue-Huapi. Sediments now recognized as the Eocene –Oligocene Vera Member of the Sarmiento formation unconformably overlie the pinkish carbonate paleosol of the Bartonian Rosado Member and clastic rocks of the Priabonian Lower Puesto Almendra Member. The Vera Member is lens-shaped in outcrop, varying in thickness along strike up to a maximum of ~90 m (Bellosi, 2010b). Largely homogeneous in appearance, the Vera Member comprises massive to poorly bedded pale yellow (Munsell 10YR8/2) to pinkish white (5YR8/2) mudstone with rare bentonite beds and paleosol intervals (Bellosi, 2010a). Although root voids and bioturbation are visible in places within the Vera Member, no erosional surfaces are readily apparent. This suggests that deposition was nearly continuous from at least 34.285 to 33.232 Ma (Dunn et al., 2013). The well-cemented, fossiliferous La Cancha bed (~48-51 m above the base of the Vera Member) is a conspicuous, laterally continuous feature in the Vera Member. A sandy deposit containing cross-beds and abundant *Coprinosphaera* ichnofossils crops out at the same stratigraphic level as the La Cancha bed ~150 m to the east of the main sampling transect of this study. We interpret this sandy deposit as a fluvial channel facies of the Vera Member.

Samples used for sedimentology and phytolith analysis in this study were taken along a transect through the Vera Member with a stratigraphic spacing of 2-4 m between sampling sites. The transect described here is Profile M of Dunn et al. (2013) and Strömberg et al. (2013), which is one of the thickest and most complete exposures of the Vera Member. Our profile (base of lower section: 45°S 43'21.0026" 68°W 40'58.2018", top of lower section: 45°S 43'36.8287" 68°W 40'55.8461", base of upper section: 45°S 43'39.3468" 68°W 41'13.9796", top of upper section: 45°S 43'40.9270" 68°W 41'10.9880" is roughly equivalent to Profile M sampled by Ré et al. (2010) albeit with a lateral offset towards Profile L, and extends Simpson’s (1930) Profile M above the level of the La Cancha interval. Although we did sample the sandy facies in the La Cancha bed (45°S 43'32.2445" 68°W 40'51.9397") as well as in the La Cancha tuff in Profile K (45°S 43.14119' 68°W 42.04163'), we restrict our study to the M profile of Dunn et al. (2013).

For this study, one sample was collected per site. Samples were collected during two field seasons (2009, 2010), with samples from the 2010 season collected to fill stratigraphic gaps between samples from the 2009 season. Magnetic properties were measured on the samples collected in 2009, and major element geochemistry was measured on a representative subset of the 2009 and 2010 samples.

Particle Size Analysis and Percent Carbonate

Particle sizes were measured at the University of Washington Tacoma. For particle size analysis, ~2 g of lightly crushed sediment samples were acidified (0.1M acetic acid) to remove carbonate cements. Carbonate-free sediments were then rinsed with deionized water and dispersed using sodium hexametaphosphate. Particle size distributions were measured on the dispersed material using a Coulter LS-200 laser particle size analyzer.

Acid treatment to remove carbonate allowed us to quantify the amount of (dry) mass lost during treatment, which we used to determine carbonate concentrations.

Phytoliths

Phytolith extraction followed standard methods (see Strömberg, 2004). Approximately one gram of sediment was crushed and treated with concentrated hydrochloric acid to dissolve carbonates. The >250 micrometer fraction was removed through sieving, and the boiled with Schultze's solution (nitric acid + potassium chlorate) to remove any organic material. The sample was further disaggregated through sieving through a 53-micrometer sieve (with fractions >53 microns and <53 microns recombined); clays were removed through repeated washing, centrifuging, and decanting. Biosilica (and other lighter components, e.g., volcanic ash) were separated from non-biogenic minerals (e.g., quartz, feldspar) using heavy liquid consisting of zinc bromide dissolved in hydrochloric acid + water with a specific gravity of 2.38. The biosilica yield was washed and dried out in ethanol and then mounted on slides in a plastic medium (Meltmount) with a refractive index of 1.539. A general vegetation analysis was published for 13 out of the 23 phytolith assemblages described herein (Strömberg et al., 2013). This work demonstrated that Vera samples tend to contain extremely low frequencies of grass silica short cell phytoliths (GSSC), hence it was not considered necessary to analyze GSSCs in immersion oil for the purpose of this study.

Phytolith identification, counting, and analysis followed Strömberg et al. (2013). Accordingly, at least 200 diagnostic phytoliths, namely forest indicator (FI; see below) or GSSC phytoliths, were identified to ensure statistical robustness of the results (Strömberg, 2009). FI morphotypes are typically produced by various forest indicator taxa (palms, woody and herbaceous dicotyledonous angiosperms, conifers, and non-seed plants such as ferns and lycophytes) (for references, see Strömberg, 2004; Strömberg et al., 2013). The abundance of grass in vegetation was determined as the relative percentage of GSSCs of diagnostic forms (FI + GSSC). We looked further at the composition of FI phytoliths to interpret vegetation type. Because GSSCs were overall so rare in the assemblages from the Vera Member, we did not analyze in detail the composition of the GSSC assemblages. The abundance of diatom frustules, sponge spicules, and chrysophyte cysts relative to diagnostic plant phytoliths from plants, as well as the relative abundance of biosilica from aquatic plants (e.g., sedges) were used to indicate the proximity of lakes or rivers to the sampling site (Strömberg, 2004, 2005).

Magnetic Properties

For magnetic analyses, ~0.2 g lightly crushed sediment was packed tightly into #4 gelcaps along with nonmagnetic foam. Low-field bulk magnetic susceptibility was measured in a Bartington dual-frequncy susceptometer at UW Tacoma. Curie temperatures were evaluated using the second derivative (Tauxe et al., 2010) of temperature-dependent susceptibility data from an AGICO Kappabridge KLY-3 at Western Washington University (WWU). Magnetic hysteresis, IRM acquisition spectra, and DC demagnetization curves were measured in fields of up to 1 T using a Princeton Measurements Micromag 3900 vibrating sample magnetometer at WWU. Full hysteresis loops were measured, including initial curves. Hysteresis loops appeared to close in fields << 1 T, so high-field slope was measured on M-H data above 700 mT. IRM acquisition spectra were measured using a logarithmic step sequence with either 25 or 75 steps and analyzed using both unconstrained and constrained log-Gaussian fits (Robertson and France, 1994; Kruiver et al., 2001; Geiss and Zanner, 2006).

Two factors that are not discussed in the manuscript informed our component analysis and our interpretation of it, although they are not essential to either one. First, hysteresis data imply that the burned loesses contain a mixture of single-domain and multidomain magnetic particles, and that the unburned loess contains additional material we believe to be superparamagnetic. However, loops characteristic of overlapping coercivity spectra (distinctly wasp-waisted, goosenecked, or potbellied hysteresis loops) were not observed. Second, the high-coercivity component recognized in IRM spectra has a higher median coercivity in specimens from the burnt intervals. Indeed, the high-coercivity component has a median coercivity that varies with the IRM magnitude of the low-coercivity component, such that the stronger the IRM of the low-coercivity component, the lower the coercivity is of the high-coercivity component. This is consistent with the interpretation that the low-coercivity component is produced by decomposing hematite.

References Cited

Bellosi, E., 2010a, Loessic and fluvial sedimentation in Sarmiento Formation pyroclastics, middle Cenozoic of Patagonia, *in* The Paleontology of Gran Barranca: Evolution and Environmental Change through the Middle Cenozoic of Patagonia, Cambridge Univer, Cambridge, p. 278–292.

Bellosi, E., 2010b, Physical stratigraphy of the Sarmiento Formation (middle Eocene - lower Miocene) at Gran Barranca, central Patagonia, *in* Madden, R., Carlini, A.A., Vucetich, M., and Kay, R.F. eds., The paleontology of Gran Barranca : evolution and environmental change through the middle Cenozoic of Patagonia, Cambridge University Press, New York, p. 19–31.

Dunn, R.E., Madden, R.H., Kohn, M.J., Schmitz, M.D., Stromberg, C.A.E., Carlini, A.A., Re, G.H., and Crowley, J., 2013, A new chronology for middle Eocene-early Miocene South American Land Mammal Ages: Geological Society of America Bulletin, v. 125, no. 3-4, p. 539–555, doi: 10.1130/B30660.1.

Geiss, C.E., and Zanner, C.W., 2006, How abundant is pedogenic magnetite? Abundance and grain size estimates for loessic soils based on rock magnetic analyses: Journal of Geophysical Research, v. 111, no. B12, doi: 10.1029/2006JB004564.

Kruiver, P.P., Dekkers, M.J., and Heslop, D., 2001, Quantification of magnetic coercivity components by the analysis of acquisition curves of isothermal remanent magnetisation: Earth and Planetary Science Letters, v. 189, no. 3-4, p. 269–276, doi: 10.1016/S0012-821X(01)00367-3.

Ré, G.H., Geuna, S.E., and Vilas, J.F., 2010, Paleomagnetism and magnetostratigraphy of Sarmiento Formation (Eocene-Miocene) at Gran Barranca, Chubut, Argentina, *in* Madden, R., Carlini, A.A., Vucetich, M., and Kay, R.F. eds., The paleontology of Gran Barranca : evolution and environmental change through the middle Cenozoic of Patagonia, Cambridge University Press, New York.

Robertson, D.J., and France, D.E., 1994, Discrimination of remanence-carrying minerals in mixtures, using isothermal remanent magnetisation acquisition curves: Physics of the Earth and Planetary Interiors, v. 82, p. 223–234, doi: 10.1016/0031-9201(94)90074-4.

Simpson, G.G., 1930, Scarritt-Patagonia Expedition Field Notes. http://research.amnh.org/paleontology/notebooks/simpson-1930a/

Tauxe, L., Butler, R.F., Van der Voo, R., and Banerjee, S.K., 2010, Essentials of paleomagnetism: University of California Press, Berkeley.

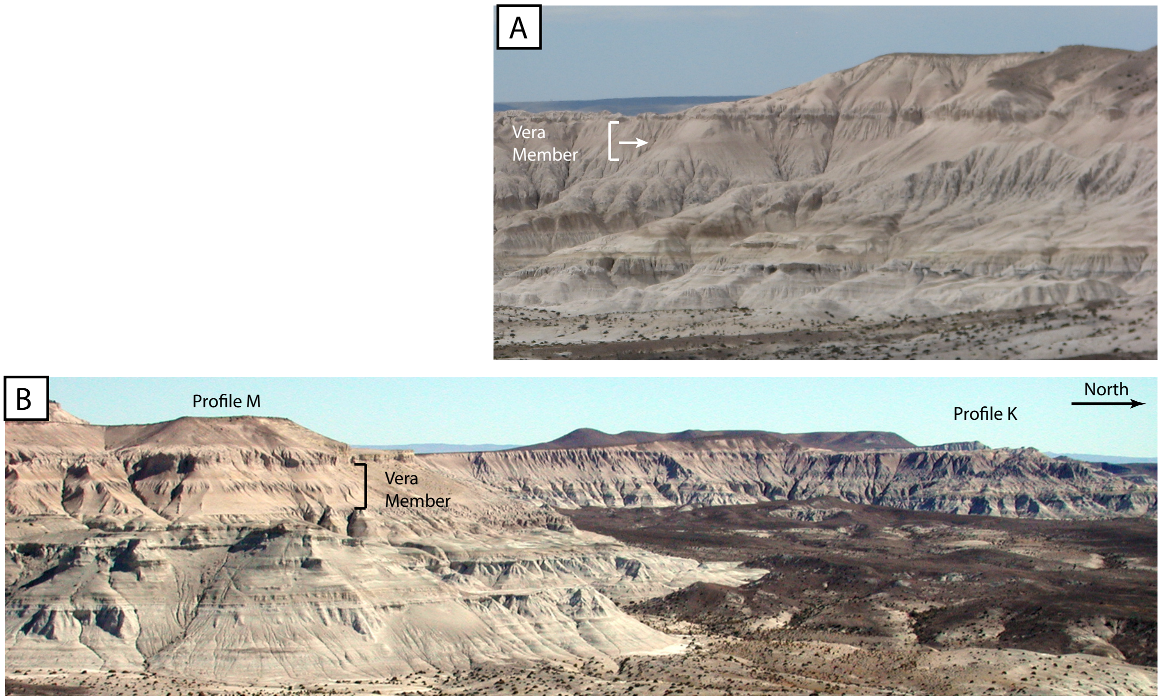

Figure DR1. Exposures of the Vera Member of the Sarmiento Formation at -
Gran Bar ranca, central Chubut Province, Argentina. A) The Vera Member at Profile K. Arrow indicates fossiliferous La Cancha bed. B) Vera Member between Profiles M and K looking to the west.

PHYTOLITH TAPHONOMY AND THE VERA MEMBER—WHERE DO THE PHYTOLITHS COME FROM?

Background on phytoliths and wind transport

Once phytoliths have been incorporated in soils they behave much like silt particles and are subject to wind transport, sometimes as far as hundreds of kilometers (e.g., Locker and Martini, 1986; Piperno, 2006; Osterreith et al., 2009). The extent to which phytoliths (and clastic grains) move laterally through eolian processes varies depending on the openness of vegetation. Closed habitats with little wind result in very little lateral movement, hence local deposition of phytoliths, and open habitats where winds tend to be strong result in regional mixing of phytolith assemblages (e.g., Piperno, 1988). Using a new phytolith-based proxy for openness (Dunn et al., 2015), we have inferred that vegetation during Vera time was very open, meaning that it is likely that Vera phytolith assemblages were influenced by long-distance transport of phytoliths throughout the study interval. That said, most studies show that local vegetation will majorly determine phytolith assemblage composition and that local differences in vegetation are distinguishable based on phytoliths, even in open vegetation where wind transport is important (Fredlund and Tieszen, 1994; Alexandre et al., 1997; Barboni et al., 1999; Kerns et al., 2001; Bremond et al., 2005; Osterreith et al., 2009; Mercader et al., 2011).

Are the Vera assemblages dominated by wind-transported phytoliths?

Because the phytolith assemblages of the Vera Member are composed mainly of palm phytoliths, which are small grains, in the 5-15(-20) micrometer size range, we hypothesize that the high abundance of palms may be related to size sorting during wind transport.

Test: To test this hypothesis, we looked at whether the relative abundance of palms is correlated with the relative abundance of the relevant grain size fraction (5-15 micrometers; hereafter referred to as D5-15) in several ways. To account for the fact that the residuals of the data are not normally distributed we square-root-transformed them before conducting parametric statistical tests (Pearson's product-moment correlation) as is recommended for count data (McDonald, 2014). We also performed non-parametric tests (Spearman rank correlation, Kendall rank correlation); in some cases where there were one or more ties in the data, resulting in imprecise p-values using these methods, we also calculated a Goodman and Kruskall’s Gamma statistic, which is less sensitive to this problem (e.g., Ritchey, 2007). To compare only samples from the same facies, we excluded PB24838 (47.9 m in section) from the analysis. This sample comes from a horizon, the only one in the Vera Member, with carbonate nodules indicative of a longer period of paleosol development, and it formed an outlier in many of the analyses (see text and Fig. 2). R statistical software (R Core Team, 2014) was used for all analyses.

Results: All analyses failed to reject the null hypothesis that there is no relationship between grain size and palm phytolith relative abundance (DR6), indicating that the assemblage composition is not simply driven by allochthonous phytolith input. Based on this we argue that local vegetation was the main source of phytoliths for all samples.

Is the variation in “burnt” palm phytoliths a result of variation in wind-transport (regional mixing)?

Studies have shown that phytoliths released from burning vegetation directly to the air have the ability to travel very far (e.g., Wallis, 2001; Piperno, 2006). These findings suggest that, in an area with a lot of fire, phytoliths will contribute disproportionally to the aerosol of silt-sized particles (that is, the regional flux of wind-borne phytoliths relative to sediment would increase), and the input of phytoliths in general to a soil would increase as a result. For this reason, we hypothesize that there will be higher concentrations of phytoliths in the soil/sediment (assuming ~constant sediment accumulation rates) in which we find high relative abundances of burnt palms. We also hypothesize that wind regime (wind speed, number of windy days etc.) has a similar effect on the relative abundance of phytoliths released from burning vegetation and the relative abundance of the 5-15 micrometer fraction of sedimentary particles in the soil.

Test: To test the relationship between blackened (“burnt”) palm phytoliths (of the total palm phytoliths) and relative abundance of phytoliths in the soil/sediment, we first estimated phytolith yield as the volume of extracted phytoliths per gram sediment processed (mm^2/g). Specifically, we measured the thickness of the yield in the glass vials and multiplied by the internal area of the vials; note that these estimates are approximate. We then tested for correlation between the relative abundance of blackened (“burnt”) palm phytoliths (BP) and phytolith yield using the same parametric and non-parametric statistical tests described above, again excluding PB24838 (47.9 m in section) from the analysis. As with the analyses of grain size (D5-15) vs. percent palm phytoliths, Gamma statistics were used when there were ties in the data. We further divided the dataset into samples from levels where markers of (weak) soil formation (e.g., root traces) were observed in the field, and conducted the same analyses separately on samples from weakly developed paleosols (SO) and samples from levels lacking any soil characteristics (NSO). Note that the sample size for the SO dataset is very small (n=7).

To test to what extent grain size distribution and percentage of blackened palm phytoliths changed in parallel, we also analyzed the relationship between D5-15 (we also studied 30-100

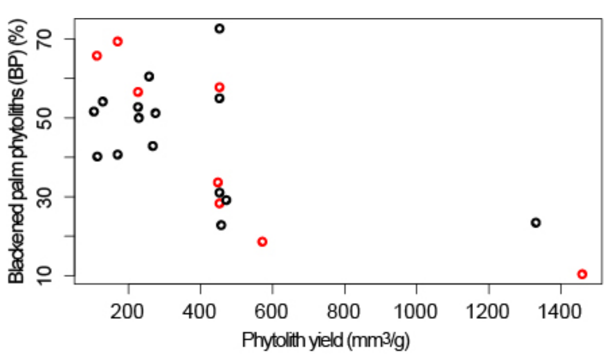

micrometer fraction; data not shown), and BP.

Figure DR2. There is a significant, strong, negative relationship between relative abundance of blackened palm phytoliths (BP) and phytolith yield. Note that samples from levels with weak signs of soil formation

(SO; red circles) and samples from levels lacking these signs (NSO; black circles) span the same range of BP and phytolith yield.

Results: For all samples taken together, phytolith yield is significantly lower in samples with abundant burnt palm phytoliths (DR6, Fig. DR5-1). When samples are split up into levels with some indications of soil processes (SO) and those without (NSO), we found that for NSO samples, there was no significant correlation between phytolith yield and relative abundance of burnt palm phytoliths, whereas for SO samples, a significant, strong, negative correlation exists (DR6). These patterns reject our hypothesis that wind transported phytoliths resulting from regional fires would add extra phytoliths to the paleosols.

What could these patterns instead indicate? The variation in relative abundance of phytoliths in the soils/sediment in general can be assumed to result either from (1) variation in local/regional primary productivity (given that the plant taxa represented in the phytolith record do not appear to change), and/or (2) variation in (eolian) sedimentation rates between samples and with that, variation in the influx of regionally derived phytoliths. Variation in primary productivity would be linked primarily to variation in temperature and evapotranspiration, which depends mainly on precipitation, precipitation seasonality, temperature, and soils (e.g., Churkina and Running, 1998). Current evidence point to relatively stable climates both in terms of temperatures and precipitation/precipitation seasonality from the middle Eocene to early Oligocene (Kohn et al., 2004; Dunn et al., 2015), but the temporal resolution is insufficient to rule out short-term variation. That said, we also see very little variation in the presence of diatoms and other biosilica that would signal a difference in environmental moisture (DR3).

Grain size analysis reveals marked differences in the fine fractions through the Vera section (DR4), pointing to variation in the eolian contribution, and therefore also potentially sedimentation rates. Could this pattern be driving BP? Across all samples, statistical analyses reveal no significant correlation between BP and D5-15, and there is also no difference in the appearance of the finer fractions (silt, clay) in thin section among samples. This in combination with the lack of significant correlation between phytolith yield and BP during times when there is no evidence of soil formation (NSO data) suggests that the percentage of burnt palm phytoliths reflect primarily variation in local (to regional) fire regime, rather than changes in relative input of eolian material.

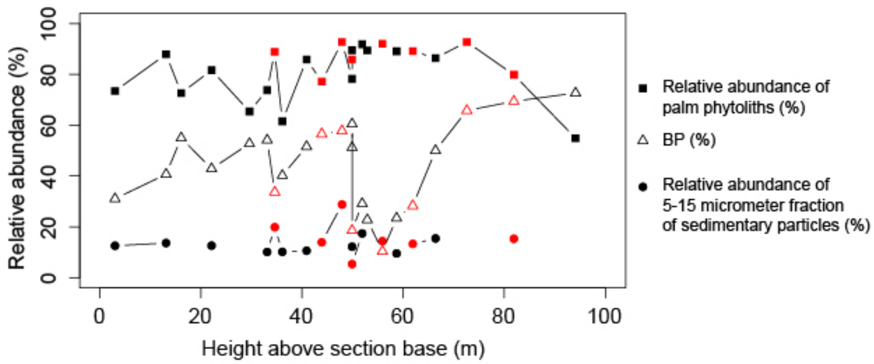

Figure DR3. Relative abundance of palms (% of total diagnostic phytoliths), blackened palms (BP; % of total palm phytoliths), and 5-15 micrometer fraction of sedimentary particles (%) through the Vera Member section. Red symbols = samples from levels with weak signs of soil formation (SO); black symbols = samples from levels without such signs (NSO).

The very strong, negative correlation between phytolith yield and blackened palm phytoliths shows that intervals when sedimentation slowed down enough to promote (some) soil formation coincided with less input of burnt palm phytoliths into the soil. We attribute this decrease in sedimentation rates to changes in wind patterns. One might therefore argue that the change in BP simply reflects less long-distance transport of burnt phytoliths. However, the fact that the shift in BP is clear in both SO and NSO samples (Fig. DR5-2) rejects this hypothesis and suggests, again, that BP records a local-regional change in fire regime. The spread and intensity of fire in modern ecosystems depends strongly on wind patterns (e.g., Linn and Cunningham, 2005); thus, we propose that altered wind patterns after Oi-1 that led to changes in sedimentation also promoted a less intense fire regime across the region.

In sum, the coincidence between changes in BP with variation in magnetite, a locally formed fire proxy, strongly points to altered fire regime in the Gran Barranca (local) area as an explanation of the observed patterns.

References:

Alexandre, A., Meunier, J.-D., Lezine, A.-M., Vincens, A., and Schwartz, D., 1997, Phytoliths: indicators of grassland dynamics during the late Holocene in intertropical Africa: Palaeogeography, Palaeoclimatology, Palaeoecology, v. 136, p. 213-229.

Barboni, D., Bonnefille, R., Alexandre, A., and Meunier, J.-D., 1999, Phytoliths as paleoenvironmental indicators, West Side Middle Awash Valley, Ethiopia: Palaeogeography, Palaeoclimatology, Palaeoecology, v. 152, p. 87-100.

Bremond, L., Alexandre, A., Hély, C., and Guiot, J., 2005, A phytolith index as a proxy of tree cover density in tropical areas: Calibration with Leaf Area Index along a forest–savanna transect in southeastern Cameroon: Global and Planetary Change, v. 45, p. 277-293.

Churkina, G., and Running, S. W., 1998, Contrasting climatic controls on the estimated productivity of global terrestrial biomes: Ecosystems, v. 1, no. 2, p. 206-215.

Dunn, R. E., Strömberg, C. A. E., Madden, R. H., Kohn, M. J., and Carlini, A. A., 2015, Linked canopy, climate and faunal evolution in the Cenozoic of Patagonia: Science, v. 347, no. 6219, p. 258-261.

Fredlund, G. G., and Tieszen, L. L., 1994, Modern phytolith assemblages from the North American Great Plains: Journal of Biogeography, v. 21, p. 321-335.

Kerns, B. K., Moore, M. M., and Hart, S. C., 2001, Estimating forest-grassland dynamics using soil phytolith assemblages and $d^{13}C$ of soil organic matter: Ecoscience, v. 8, no. 4, p. 478-488.

Kohn, M. J., Josef, J. A., Madden, R., Kay, R., Vucetich, G., and Carlini, A. A., 2004, Climate stability across the Eocene-Oligocene transition, southern Argentina: Geology, v. 32, no. 7, p. 621-624.

Kohn, M. J., Strömberg, C. A. E., Madden, R. H., Dunn, R. E., Evans, S., Palacios, A., and Carlini, A. A., in review, Quasi-static Eocene-Oligocene climate in Patagonia promotes slow faunal evolution and mid-Cenozoic global cooling: Palaeogeography Palaeoclimatology Palaeoecology.

Linn, R. R., and Cunningham, P., 2005, Numerical simulations of grass fires using a coupled atmosphere—fire model: Basic fire behavior and dependence on wind speed, Journal of Geophysical Research, Volume 110.

Locker, S., and Martini, E., 1986, Phytoliths from the southwest Pacific Site 591: Initial reports of the Deep Sea Drilling Program, v. 90, p. 1079-1084.

McDonald, J. H., 2014, Handbook of Biological Statistics, Baltimore, Maryland, Sparky House Publishing.

Mercader, J., Bennett, T., Esselmont, C., Simpson, S., and Walde, D., 2011, Soil phytoliths from miombo woodlands in Mozambique: Quaternary Research, v. 75, no. 1, p. 138-150.

Osterrieth, M., Madella, M., Zurro, D., and Alvarez, M. F., 2009, Taphonomical aspects of silica phytoliths in the loess sediments of the Argentinean Pampas: Quaternary International, v. 193, p. 70-79.

Piperno, D. R., 1988, Phytolith Analysis, an Archaeological and Geological Perspective, San Diego, Academic Press, 280 p.:

Piperno, D. R., 2006, Phytoliths: a comprehensive guide for archaeologists and paleoecologists New York, AltaMira Press, 304 p.:

Ritchey, F. J., 2007, The Statistical Imagination: Elementary Statistics for the Social Sciences, McGraw-Hill Humanities.

Team, R. C., 2014, R: A Language and Environment for Statistical Computing, R Foundation for Statistical Computing, Vienna, Austria.

Wallis, L. A., 2001, Environmental history of northwest Australia based on phytolith analysis at Carpenter's Gap 1: Quaternary International, v. 83-85, no. 2001, p. 103-117.

Table DR1. Phytolith assemblage data.

				biogenic silica[5]			Phytolith morphotypes, rel. abundance of total count (%)[6]										Tree cover[7]		diagnostic forms[8]			Burnt palm (BP)[9]		
								Forest indic.		GSSC														
UWBM[2] no.	Meter level in section	Age[3]	Preservation[4]	Diatoms	Chrysophyte cysts	Sponge spicules	AQ	PALM	Other FI	CH TOT	POOID TOT	PACMAD	OTHG	NDG	NDO	Total phytolith count	FI-t	FI-t ratio 95% C.I. (%)	Pooideae	PACMAD	Danthonioideae?/ Bambusoideae?	BP=100*PALM$_{bu}$/PALM (%)	BP 95% C.I. (%)	BP count size
PB18443	3	35.15342	G (alt, fra)	n.o.	n.o.	n.o.	0	71	25	0	0.5	0	0	0.9	1.9	422	99.3	98.3-100	CE-1	n.o.	p	31	22.4-39.7	116
PB18444	13	34.81480	G	n.o.	n.o.	n.o.	0	80	10	0	0.3	0.1	0	1.1	7.5	280	99.2	98.0-100	CE-1	n.o.	p?	41	32.2-50.0	118
PB18445	16	34.71421	G (alt, fra)	n.o.	n.o.	p	0	71	27	0	0	0.1	0	0.9	1.5	550	99.8	99.4-100	CE-1	n.o.	p	55	45.9-64.0	111
PB18446	22	34.51305	G (alt)	n.o.	n.o.	n.o.	0	77	17	0	0.3	0.1	0	0	5.5	363	99.1	98.0-100	CE-1	n.o.	p	43	34.5-52.1	119
PB18447	30	34.26160	G (alt)	n.o.	n.o.	n.o.	0	63	33	0	0	0	p	1.9	2.1	376	100	N/A	n.o.	n.o.	n.o.	53	43.6-61.8	110
PB28470	33	34.144254	G (alt)	p	n.o.	n.o.	0	56	19	0	0.4	0	0	3.2	21	277	99	97.6-100	n.o.	n.o.	n.o.	54	45.9-62.4	133
PB18448	35	34.09396	G (alt)	n.o.	n.o.	p	1	86	11	0	0	0	0	0.5	2.1	382	100	N/A	n.o.	n.o.	p	34	25.0-42.2	116
PB18449	36	34.04367	G (alt)	n.o.	p	n.o.	0	59	37	0	0.1	0.1	0	1.4	2.5	441	99.8	99.3-100	BI-1	n.o.	n.o.	40	30.8-49.5	107
PB24837	41	33.882743	G-P (alt)	p	n.o.	n.o.	0	64	11	0	0	0	0	3.2	22	283	100	N/A	n.o.	n.o.	n.o.	52	42.9-60.3	126
PB18450	44	33.78216	G (alt)	n.o.	n.o.	n.o.	p	62	17	0.1	0.2	0.2	1	2.6	17	273	98.2	96.3-99.6	n.o.	BI-5	n.o.	57	47.5-65.6	122
PB24838	48	33.648054	G (alt)	n.o.	n.o.	n.o.	0.4	81	6.3	0	0	0	0	3.4	8.9	237	100	N/A	n.o.	n.o.	n.o.	58	48.3-66.4	116
PB18451	50	33.581 (La	G (alt)	p	mab	p	0	73	12	0	0	0	0	0.7	14	283	99.6	98.7-100	n.o.	n.o.	n.o.	19	11.5-26.5	113
PB18452	50	Cancha	G (alt)	n.o.	n.o.	p	0	75	21	0	0	0	0	0.9	2.8	458	100	N/A	n.o.	n.o.	p?	51	42.4-60.0	125
PB24839	50	tuff)	VG (alt)	p	n.o.	p	0	79	8.4	0	0.4	0	0	0.8	11	238	99	97.6-100	n.o.	n.o.	n.o.	60	51.6-69.4	124
PB24840	52	33.569209	G (alt)	p	n.o.	n.o.	0.4	81	7.2	0	0	0	0	0.8	11	237	100	N/A	n.o.	n.o.	n.o.	29	21.3-37.0	127
PB24841	53	33.551524	G-P (alt)	p	n.o.	n.o.	0	77	7.2	0	0.8	0	1	3.8	11	265	97.8	95.7-99.6	CE-1	n.o.	n.o.	23	16.2-30.1	136
PB24842	56	33.51851	G-P (alt)	p	n.o.	n.o.	0	78	4.7	0	0.8	0.4	1	2.1	13	236	97.5	95.1-99.5	n.o.	SA-2?	n.o.	10	5.17-16.4	116
PB24843	59	33.49375	G (alt)	p	n.o.	n.o.	0.4	71	8	0	0.8	0	0	1.5	18	263	99	97.6-100	n.o.	n.o.	n.o.	23	16.3-30.5	141

PB18453 62	33.44069	P (et)	n.o.	n.o.	n.o.	0	65	8	0	0	0	0	2.4	24	289	100	N/A	n.o.	n.o.	n.o.	28	19.8-36.8	106
PB18454 66	33.39530	G (alt)	n.o.	p	n.o.	0	71	10	0.4	0	0	0	1.8	16	279	99.1	97.7-100	n.o.	n.o.	n.o.	50	40.9-59.1	110
PB24844 73	33.35875	VG (alt)	n.o.	n.o.	n.o.	0	76	5.1	0	0.4	0	0	6.7	12	254	99.0	97.5-100	n.o.	n.o.	n.o.	66	60.3-71.2	292
PB24845 82	33.30392	VG (alt)	p	n.o.	n.o.	0.4	63	15	0	0	0	1	3.7	18	272	98.6	96.7-100	n.o.	n.o.	n.o.	69	63.7-75.1	245
PB18455 94	33.23200	G (alt)	p	p	p	0.3	32	17	0	5.8	0.6	2	8.2	34	392	85.0	80.2-89.7	BI-1,	BI-5, SA-6	n.o.	73	64.1-80.3	117

[1]N/A = not applicable.

[2]UWBM = University of Washington Burke Museum of Natural History and Culture.

[3]Age model, see Dunn et al. (2013) and Strömberg et al. (2013).

[4]G = good-pristine (occluded organic material and fine ornamentation routinely preserved on GSSC; elongates and bulliform cells may be etched or broken); P = poor (occluded material often missing and GSSC commonly broken or etched; elongates and bulliform cells often etched or broken); VP = very poor (phytoliths fragmentary or structurally/texturally altered to such a degree that identification is complicated); alt = altered; et = etched, fra=fragmented.

[5]Semiquantitative estimation: n.o. = not observed; p = present (rare); mab = moderately abundant; ab = abundant; vab = very abundant.

[6] AQ = phytoliths from wetland plants (e.g, *Equisetum* , sedges); other FI = morphotypes typical of forest indicators (woody and herbaceous dicotyledons, ferns, conifers); NDG = non-diagnostic (potential) grass phytoliths (e.g., cuneiform bulliforms, elongate sinuous, echinate, and dendritic, acicular hair base); NDO = non-diagnostic and indeterminable phytoliths. For other definitions, see Strömberg et al. (2013) and text.

[7]Tree cover is estimated using a rough proxy: FI-t = 100*(PALM + Other FI)/(PALM + Other FI + GSSC).

[8]Particularly diagnostic GSSC morphotypes: BI-1 = *Stipa* -type bilobate; BI-5 = simple lobate bilobate; CE-1 = crenate with symmetry A; SA-2 = almost true saddle; SA-6 = saddle-bilobate (Z-axis); n.o. = not observed; p = present; ab = abundant. See Strömberg et al. (2013); full description of morphotypes in Strömberg (2003).

[9]BP = Percentage of palm phytoliths that show clear signs of alteration possibly due to burning (dark centers, black bubbles, "melted" surface). See text.

Table DR2

ID	UWBM no.	Position	Age	Mass	Mean	Mode	Median	SD	CV	Variance	Skew	Kurtosis
ARG10-059	PB29103	1.5	35.2037094	NA	82.2979	153.824	56.5199	79.9347	97.1285	6389.56	1.52688	2.7105
SGB09-133	PB18443	3	35.1534188	0.0003421	57.2431	50.2242	44.4965	47.5549	83.0753	2261.47	0.976309	0.233628
ARG10-060	PB29104	4.5	35.1031283	NA	84.2551	140.125	67.4988	72.4277	85.9623	5245.77	1.37522	2.81052
SGB09-134	PB28466	6	35.0528377	0.0002956	52.7706	45.7513	39.7027	45.9044	86.9885	2107.21	1.15157	0.703401
ARG10-061	PB29105	7.7	34.9958417	NA	48.0993	41.6768	32.8236	46.5586	96.7968	2167.7	1.32359	1.02817
SGB09-135	PB28467	9.4	34.9388457	0.0002769	95.4124	127.646	80.5528	74.8121	78.4092	5596.85	1.35081	2.68198
ARG10-062	PB29106	11.25	34.8768206	NA	41.719	37.9651	25.4537	44.9286	107.693	2018.58	1.49441	1.58011
SGB09-136	PB18444	13.1	34.8147956	0.0003076	90.5558	41.6768	44.6883	123.538	136.422	15261.5	2.78149	9.89081
ARG10-063	PB29107	15.1	34.7477415	NA	41.3321	37.9651	26.9108	43.3661	104.921	1880.62	1.55898	1.88486
ARG10-064	PB29108	17.1	34.6806874	NA	41.7567	41.6768	28.4649	41.9696	100.51	1761.44	1.42972	1.5083
SGB09-138	PB28468	19.1	34.6136333	0.0002997	38.7926	37.9651	25.6673	40.924	105.494	1674.77	1.70671	2.52972
ARG10-065	PB29109	20.6	34.5633427	NA	48.4676	41.6768	32.4253	47.6038	98.2177	2266.12	1.26632	0.783164
SGB09-139	PB18446	22.1	34.5130521	0.000347	68.16	140.125	47.1011	66.7816	97.9776	4459.78	1.82144	4.82768
ARG10-066	PB29110	23.6	34.4627615	NA	41.4455	37.9651	27.1005	43.1903	104.21	1865.4	1.50531	1.67413
SGB09-140	PB28469	25.6	34.3957074	0.0003093	62.3986	50.2242	48.9791	50.6771	81.2151	2568.17	0.888816	-0.0054133
ARG10-068	PB29112	31.6	34.1945451	NA	65.768	87.8959	54.865	50.1117	76.1946	2511.18	0.746913	-0.212409
SGB09-142	PB28470	33.1	34.1442545	0.0003086	73.0759	140.125	60.7389	56.4517	77.2508	3186.8	0.661222	-0.475859
ARG10-069	PB18488	34.6	34.0939639	NA	51.94	140.125	33.4467	50.2443	96.7353	2524.49	1.07766	0.152834
ARG10-070	PB29113	36.1	34.0436733	NA	59.4395	45.7513	42.8437	52.7349	88.7204	2780.97	0.99623	0.0856545
SGB09-143	PB18449	36.1	34.0436733	0.0003056	66.9009	80.068	54.3406	52.4206	78.3556	2747.92	0.777302	-0.215869
SGB09-144	PB28471	37.9	33.9833246	0.0002883	55.4378	50.2242	43.9199	45.1335	81.4129	2037.04	1.03998	0.510543
SGB09-145	PB24837	40.9	33.8827435	0.0001718	79.3835	50.2242	51.942	95.6098	120.44	9141.23	3.82051	22.9338
SGB09-146	PB18450	43.9	33.7821623	0.0002713	55.4222	45.7513	40.6541	48.7925	88.0377	2380.71	1.03747	0.247653
SGB09-150	PB24838	47.9	33.6480541	0.0003266	29.7773	18.0016	17.1532	36.3163	121.96	1318.87	2.20526	4.80614
SGB09-151	PB28475	48.9	33.614527	0.0003246	79.4281	37.9651	33.698	107.405	135.223	11535.9	2.21919	5.16254
SGB09-152	PB28476	49.9	33.581	0.0003209	75.8288	50.2242	50.8671	78.5615	103.604	6171.91	2.15595	6.0355
SGB09-158	PB24839	49.9	33.581	0.000297	94.3172	140.125	61.6659	95.8902	101.668	9194.92	1.53704	2.42988
ARG10-076	PB24840	51.9	33.5692094	NA	54.0474	127.646	37.3377	50.3437	93.1475	2534.49	0.963957	-0.0490142
SGB09-159	PB28479	54.5	33.5361959	0.0003599	57.387	72.9373	54.628	37.6307	65.5735	1416.07	0.457708	-0.372113
SGB09-154	PB24842	55.9	33.5185101	0.0003924	58.3887	140.125	43.8393	50.3137	86.1702	2531.47	0.896772	-0.109771
ARG10-077	PB29119	56.5	33.5067196	NA	50.3829	72.9373	42.5719	40.5958	80.5746	1648.02	0.731001	-0.262845
SGB09-160	PB24843	58.7	33.49375	0.0003386	57.9355	72.9373	53.9468	38.8263	67.0163	1507.48	0.517055	-0.351465
SGB09-156	PB18453	61.9	33.4406925	0.0002907	59.6842	127.646	46.6492	49.3782	82.7325	2438.2	0.816498	-0.232015
SGB09-162	PB28481	63.8	33.4283125	0.0002806	47.5298	41.6768	33.3867	44.5604	93.7525	1985.63	1.18577	0.633429
SGB09-157	PB28478	64.9	33.4106267	0.000305	88.4191	140.125	67.9815	80.1581	90.657	6425.32	1.61812	3.44406
SGB09-163	PB18454	66.4	33.395299	0.0002832	48.5915	50.2242	37.9606	42.2228	86.8932	1782.76	1.13228	0.798755
SGB09-164	PB28482	68.8	33.3811503	0.0003079	59.6742	72.9373	55.189	40.252	67.4528	1620.22	0.577346	-0.198182
SGB09-167	PB24845	81.9	33.3039223	0.0003037	79.0236	153.824	40.543	93.804	118.704	8799.18	1.93393	3.85398
SGB09-168	PB28484	86.9	33.2744459	0.0002738	81.7244	153.824	55.6606	78.3607	95.8841	6140.41	1.58611	2.969

ID	PC_Sand	PC_Silt	PC_Clay	Xlfreq	Munsell	M1	DP1	Bh1	M2	DP2	Bh2	PC_CaCO3
ARG10-059	0.49337555	0.4336125	0.07301195	NA	2.5Y 8/1	NA	NA	NA	NA	NA	NA	NA
SGB09-133	0.39469352	0.53300522	0.07230127	4.45E-07	10YR 8/1	1.07E-06	0.226547	1.53163	1.79E-06	0.563175	1.7774	0.08062275
ARG10-060	0.55058336	0.38872743	0.06068921	NA	10YR 8/1	NA	NA	NA	NA	NA	NA	NA
SGB09-134	0.34554528	0.57784612	0.0766086	6.25E-07	10YR 8/1	9.92E-07	0.226547	1.53163	1.74E-06	0.526801	1.63748	0.07986093
ARG10-061	0.29222111	0.61243938	0.09533951	NA	2.5Y 8/1	NA	NA	NA	NA	NA	NA	NA
SGB09-135	0.62625434	0.33750728	0.03623838	6.92E-07	10YR 8/1	9.20E-07	0.226547	1.53163	1.92E-06	0.402589	1.78061	0.03795531
ARG10-062	0.24320067	0.61903234	0.137767	NA	10YR 8/1	NA	NA	NA	NA	NA	NA	NA
SGB09-136	0.41928138	0.49850638	0.08221224	2.26E-08	10YR 8/1	1.44E-07	0.226547	1.53163	8.62E-07	0.422542	1.91484	0.05010712
ARG10-063	0.23051164	0.64640008	0.12308828	NA	2.5Y 8/1	NA	NA	NA	NA	NA	NA	NA
ARG10-064	0.24728602	0.63048805	0.12222593	NA	2.5Y 8/1	NA	NA	NA	NA	NA	NA	NA
SGB09-138	0.20368436	0.68027745	0.11603819	6.18E-07	10YR 8/1	9.44E-07	0.226547	1.53163	1.61E-06	0.570768	1.61776	0.05877705
ARG10-065	0.29730918	0.6029614	0.09972943	NA	2.5Y 8/1	NA	NA	NA	NA	NA	NA	NA
SGB09-139	0.42971743	0.49256353	0.07771904	1.12E-06	10YR 8/1	1.54E-06	0.226547	1.53163	3.45E-06	0.515376	1.46499	0.06760715
ARG10-066	0.23787419	0.63571897	0.12640684	NA	2.5Y 8/1	NA	NA	NA	NA	NA	NA	NA
SGB09-140	0.43241799	0.49579809	0.07178393	1.05E-06	10YR 8/1	1.25E-06	0.226547	1.53163	2.71E-06	0.534936	1.49128	0.07393592
ARG10-068	0.47922095	0.46476657	0.05601247	NA	10YR 8/1	NA	NA	NA	NA	NA	NA	NA
SGB09-142	0.51745142	0.42038993	0.06215865	2.57E-07	7.5YR 8/1	6.34E-07	0.226547	1.53163	1.07E-06	0.489215	1.82283	0.04816852
ARG10-069	0.33752045	0.56861192	0.09386763	NA	10YR 8/1	NA	NA	NA	NA	NA	NA	NA
ARG10-070	0.39073472	0.52866722	0.08059806	NA	NA	NA	NA	NA	NA	NA	NA	NA
SGB09-143	0.4759723	0.45849693	0.06553077	4.54E-07	NA	8.03E-07	0.226547	1.53163	1.28E-06	0.542532	1.69106	0.04244959
SGB09-144	0.37862781	0.55190721	0.06946498	3.22E-07	7.5YR 8/2	5.23E-07	0.226547	1.53163	8.71E-07	0.568075	1.57742	0.03386107
SGB09-145	0.46078308	0.47314088	0.06607604	3.86E-07	NA	7.43E-07	0.226547	1.53163	1.23E-06	0.515969	1.72424	0.02408982
SGB09-146	0.36754697	0.5483958	0.08405723	4.14E-07	7.5YR 8/1	7.43E-07	0.226547	1.53163	1.23E-06	0.515969	1.72424	0.03199106
SGB09-150	0.12885043	0.71536836	0.15578121	4.44E-07	7.5YR 8/1	1.02E-06	0.226547	1.53163	1.97E-06	0.593918	1.52764	0.16953987
SGB09-151	0.36114096	0.53157151	0.10728754	5.70E-07	7.5YR 8/1	7.24E-07	0.226547	1.53163	1.34E-06	0.598104	1.58109	0.11740578
SGB09-152	0.45235991	0.48431947	0.06332063	5.97E-07	7.5YR 8/1	1.02E-06	0.226547	1.53163	1.73E-06	0.566399	1.60882	0.06317064
SGB09-158	0.51529655	0.41306458	0.07163887	7.57E-07	10YR 8/1	8.46E-07	0.226547	1.53163	2.30E-06	0.508066	1.45739	0.0361462
ARG10-076	0.36745295	0.52716608	0.10538097	NA	10YR 8/1	NA	NA	NA	NA	NA	NA	NA
SGB09-159	0.46813367	0.47325362	0.05861271	5.55E-08	7.5YR 8/2	3.14E-08	0.226547	1.53163	1.90E-07	0.566313	1.85173	0.02594463
SGB09-154	0.40439197	0.51419421	0.08141383	2.01E-07	7.5YR 8/1	8.47E-09	0.226547	1.53163	3.30E-07	0.497237	1.92021	0.06315296
ARG10-077	0.38431208	0.5264126	0.08927532	NA	2.5Y 8/1	NA	NA	NA	NA	NA	NA	NA
SGB09-160	0.46329312	0.47729764	0.05940924	3.90E-08	7.5YR 8/2	6.47E-08	0.226547	1.53163	3.27E-07	0.460514	1.82964	0.03701399
SGB09-156	0.42306852	0.49984408	0.0770874	1.14E-07	7.5YR 8/1	1.39E-07	0.226547	1.53163	6.46E-07	0.449649	1.8517	0.03953718
SGB09-162	0.30258129	0.59979035	0.09762837	4.25E-07	7.5YR 8/2	1.13E-06	0.226547	1.53163	1.25E-06	0.560224	1.67558	0.02035526
SGB09-157	0.55343601	0.3937998	0.05276419	4.78E-07	7.5YR 8/1	1.11E-06	0.226547	1.53163	1.86E-06	0.613355	1.62216	0.05267374
SGB09-163	0.32757647	0.58246452	0.08995901	1.87E-07	7.5YR 8/2	7.20E-07	0.226547	1.53163	9.41E-07	0.477456	1.78977	0.0212673
SGB09-164	0.4755381	0.46395109	0.06051081	3.86E-07	NA	5.89E-07	0.226547	1.53163	8.52E-07	0.482947	1.74077	0.03842965
SGB09-167	0.39974637	0.51557459	0.08467905	7.41E-07	7.5YR 8/1	1.44E-06	0.226547	1.53163	2.15E-06	0.571957	1.49511	0.02732598
SGB09-168	0.48784687	0.45137871	0.06077442	6.27E-07	7.5YR 8/1	9.12E-07	0.226547	1.53163	1.21E-06	0.484635	1.68875	0.03038715

ID	Si	Ti	Al	Fe	Mg	Mn	Ca	Na	P	K	CIA.K	P_Sheldon
ARG10-059	NA	NA	NA	NA	NA	NA	NA	NA	NA	NA	NA	NA
SGB09-133	0.65789295	0.00861027	0.1435817	0.05258644	0.02809758	0.00066981	0.0315651	0.04263694	0.00088312	0.03347611	65.928571	809.936258
ARG10-060	NA	NA	NA	NA	NA	NA	NA	NA	NA	NA	NA	NA
SGB09-134	0.6727785	0.00763205	0.14684739	0.04840207	0.02816672	0.00078777	0.02401796	0.04414076	0.00079446	0.02643233	68.2991708	848.658074
ARG10-061	NA	NA	NA	NA	NA	NA	NA	NA	NA	NA	NA	NA
SGB09-135	0.68481134	0.00715476	0.15418122	0.04803506	0.02839324	0.00082289	0.02504792	0.02940239	0.00101886	0.02113231	73.9012051	947.679573
ARG10-062	NA	NA	NA	NA	NA	NA	NA	NA	NA	NA	NA	NA
SGB09-136	NA	NA	NA	NA	NA	NA	NA	NA	NA	NA	NA	NA
ARG10-063	NA	NA	NA	NA	NA	NA	NA	NA	NA	NA	NA	NA
ARG10-064	NA	NA	NA	NA	NA	NA	NA	NA	NA	NA	NA	NA
SGB09-138	NA	NA	NA	NA	NA	NA	NA	NA	NA	NA	NA	NA
ARG10-065	NA	NA	NA	NA	NA	NA	NA	NA	NA	NA	NA	NA
SGB09-139	NA	NA	NA	NA	NA	NA	NA	NA	NA	NA	NA	NA
ARG10-066	NA	NA	NA	NA	NA	NA	NA	NA	NA	NA	NA	NA
SGB09-140	NA	NA	NA	NA	NA	NA	NA	NA	NA	NA	NA	NA
ARG10-068	NA	NA	NA	NA	NA	NA	NA	NA	NA	NA	NA	NA
SGB09-142	NA	NA	NA	NA	NA	NA	NA	NA	NA	NA	NA	NA
ARG10-069	NA	NA	NA	NA	NA	NA	NA	NA	NA	NA	NA	NA
ARG10-070	NA	NA	NA	NA	NA	NA	NA	NA	NA	NA	NA	NA
SGB09-143	NA	NA	NA	NA	NA	NA	NA	NA	NA	NA	NA	NA
SGB09-144	0.66844969	0.00684681	0.15005952	0.04481978	0.02625391	0.02257098	0.03001817	0.02337162	0.0025103	0.02509922	73.7576947	945.00412
SGB09-145	0.68652493	0.00736453	0.15301101	0.04731375	0.0284255	0.00426897	0.02332615	0.02198683	0.00063373	0.0271446	77.1520414	1010.35589
SGB09-146	NA	NA	NA	NA	NA	NA	NA	NA	NA	NA	NA	NA
SGB09-150	0.4973942	0.00599148	0.11708765	0.03755558	0.01746327	0.00158824	0.26775351	0.02970459	0.00242223	0.02303927	28.2448074	385.517045
SGB09-151	NA	NA	NA	NA	NA	NA	NA	NA	NA	NA	NA	NA
SGB09-152	0.66916221	0.00736835	0.1479606	0.04455239	0.02270457	0.00118423	0.031186	0.04147744	0.00380549	0.03059872	67.0645852	828.266556
SGB09-158	NA	NA	NA	NA	NA	NA	NA	NA	NA	NA	NA	NA
ARG10-076	0.70431982	0.00759267	0.16067439	0.04627324	0.02230641	0.00075299	0.01960141	0.01598172	0.00163708	0.02086027	81.8691635	1108.74633
SGB09-159	NA	NA	NA	NA	NA	NA	NA	NA	NA	NA	NA	NA
SGB09-154	0.69690595	0.00823391	0.15721585	0.04697324	0.02499144	0.00037568	0.02009636	0.0197243	0.0004776	0.02500568	79.790213	1064.25457
ARG10-077	NA	NA	NA	NA	NA	NA	NA	NA	NA	NA	NA	NA
SGB09-160	NA	NA	NA	NA	NA	NA	NA	NA	NA	NA	NA	NA
SGB09-156	NA	NA	NA	NA	NA	NA	NA	NA	NA	NA	NA	NA
SGB09-162	NA	NA	NA	NA	NA	NA	NA	NA	NA	NA	NA	NA
SGB09-157	0.67091754	0.00928402	0.16040206	0.05474458	0.02466378	0.00130009	0.02554267	0.0264627	0.00101082	0.02567175	75.5162214	978.315547
SGB09-163	NA	NA	NA	NA	NA	NA	NA	NA	NA	NA	NA	NA
SGB09-164	NA	NA	NA	NA	NA	NA	NA	NA	NA	NA	NA	NA
SGB09-167	NA	NA	NA	NA	NA	NA	NA	NA	NA	NA	NA	NA
SGB09-168	0.69789156	0.00687033	0.15397372	0.04574738	0.02447553	0.00085793	0.02298693	0.01956256	0.00064276	0.02699131	78.3488723	1034.46068

ID	Mr	Ms	Mr.Ms	Hc	Hcr	Hcr.Hc	Xi	Xhf
ARG10-059	NA	NA	NA	NA	NA	NA	NA	NA
SGB09-133	8.09E-06	3.86E-05	0.2094509	0.01291862	0.03393494	2.62682392	0.00034314	5.35E-08
ARG10-060	NA	NA	NA	NA	NA	NA	NA	NA
SGB09-134	9.07E-06	5.60E-05	0.16195033	0.00947805	0.0292357	3.08457006	0.00049413	4.67E-08
ARG10-061	NA	NA	NA	NA	NA	NA	NA	NA
SGB09-135	1.05E-05	5.02E-05	0.20834711	0.01354938	0.03662566	2.70312442	0.00043289	5.71E-08
ARG10-062	NA	NA	NA	NA	NA	NA	NA	NA
SGB09-136	3.29E-06	1.30E-05	0.2539022	0.02100886	0.05581374	2.65667628	0.00012589	5.23E-08
ARG10-063	NA	NA	NA	NA	NA	NA	NA	NA
ARG10-064	NA	NA	NA	NA	NA	NA	NA	NA
SGB09-138	8.29E-06	5.06E-05	0.16384088	0.00944181	0.02856028	3.02487405	0.00044563	4.47E-08
ARG10-065	NA	NA	NA	NA	NA	NA	NA	NA
SGB09-139	1.40E-05	8.74E-05	0.16070061	0.00860675	0.02449294	2.845783	0.0007514	4.96E-08
ARG10-066	NA	NA	NA	NA	NA	NA	NA	NA
SGB09-140	1.24E-05	7.50E-05	0.16536004	0.00892895	0.02514767	2.81642057	0.00064443	4.72E-08
ARG10-068	NA	NA	NA	NA	NA	NA	NA	NA
SGB09-142	5.45E-06	2.41E-05	0.22562671	0.01496306	0.03625399	2.42289946	0.00022687	5.44E-08
ARG10-069	NA	NA	NA	NA	NA	NA	NA	NA
ARG10-070	NA	NA	NA	NA	NA	NA	NA	NA
SGB09-143	6.70E-06	3.73E-05	0.17974919	0.01073337	0.03035737	2.82831674	0.00034207	5.37E-08
SGB09-144	4.71E-06	2.85E-05	0.1651248	0.00919179	0.02708159	2.94628	0.00025441	2.87E-08
SGB09-145	5.45E-06	2.54E-05	0.21427424	0.01369812	0.0336659	2.45770223	0.0002298	4.27E-08
SGB09-146	7.15E-06	3.72E-05	0.19221794	0.01187252	0.03185932	2.68345052	0.00033573	5.46E-08
SGB09-150	8.78E-06	5.38E-05	0.16303293	0.00892804	0.02616843	2.93103862	0.0004621	4.07E-08
SGB09-151	6.12E-06	4.04E-05	0.15155259	0.00878819	0.02750138	3.12935727	0.00035403	3.85E-08
SGB09-152	8.35E-06	5.08E-05	0.16424242	0.00944116	0.02807702	2.9738939	0.00044927	5.05E-08
SGB09-158	1.04E-05	6.92E-05	0.14978897	0.00809342	0.02398524	2.96354817	0.00059816	4.81E-08
ARG10-076	NA	NA	NA	NA	NA	NA	NA	NA
SGB09-159	6.07E-07	2.94E-06	0.20605705	0.01433543	0.04878823	3.40333216	5.42E-05	4.70E-08
SGB09-154	8.40E-07	3.59E-06	0.23377123	0.01967654	0.06906234	3.50988233	5.75E-05	4.64E-08
ARG10-077	NA	NA	NA	NA	NA	NA	NA	NA
SGB09-160	1.15E-06	5.25E-06	0.21954185	0.01614512	0.04563434	2.82650981	7.77E-05	5.35E-08
SGB09-156	2.70E-06	1.10E-05	0.24526175	0.01777153	0.04716208	2.65379965	0.00011802	5.47E-08
SGB09-162	8.20E-06	3.99E-05	0.20548144	0.01192946	0.02984875	2.50210404	0.00037303	6.56E-08
SGB09-157	9.30E-06	4.96E-05	0.18737022	0.01059243	0.02888691	2.72712777	0.00044165	6.10E-08
SGB09-163	5.81E-06	2.56E-05	0.22721649	0.01445757	0.03385995	2.34202221	0.00025023	6.74E-08
SGB09-164	4.65E-06	2.37E-05	0.19671431	0.01189545	0.03254928	2.73627984	0.00023449	6.04E-08
SGB09-167	1.13E-05	7.45E-05	0.1519225	0.00870441	0.02540418	2.91854096	0.00065043	5.07E-08
SGB09-168	7.71E-06	4.17E-05	0.18497973	0.01152962	0.03032716	2.63036943	0.00037617	5.30E-08

Explanation of Columns

ID	Specimen ID from PSA filename, fixed so that it contains 3 letters, 2 numbers, a dash, and 3 numbers
Position	Stratigraphic position relative to base of Vera Member
Age	Age (Dunn et al, 2013)
Mass	Mass of sediment in g
Mean	Mean grain diameter in µm from PSA data file
Mode	Mode of grain diameters in µm from PSA data file
Median	Median grain diameter in µm from PSA data file
SD	Standard deviation in grain diameter in µm from PSA data file
CV	CV? of grain diameter in µm from PSA data file
Variance	Variance of grain diameters measured in µm from PSA data file
Skew	Skewness of grain diameters measured in µm from PSA data file
Kurtosis	Kurtosis of grain diameters measured in µm from PSA data file
PC_Sand	Sand fraction (vol % >62 µm) calculated from grain diameters measured in µm from PSA data file
PC_Silt	Silt fraction (vol % 4-62 µm) calculated from grain diameters measured in µm from PSA data file
PC_Clay	Clay fraction (vol % <4 µm) calculated from grain diameters measured in µm from PSA data file
Xlfreq	Low-frequency susceptibility (mass normalized), in m3/kg
Munsell	Munsell color
M1	Low Coercivity IRM Component, Magnetizaton (Am^2/kg)
DP1	Low Coercivity IRM Component, Dispersion Parameter (Am^2/kg)
Bh1	Low Coercivity IRM Component, Median Coercivity (Am2/kg)
M2	Moderate Coercivity IRM Component, Magnetizaton (Am^2/kg)
DP2	Moderate IRM Component, Dispersion Parameter (Am^2/kg)
Bh2	Moderate IRM Component, Median Coercivity (Am^2/kg)
PC_CaCO3	Percent carbonate (by vonlum, %o)
Si	Major elements (as oxides) determined by ICP-OES
Ti	
Al	
Fe	
Mg	
Mn	
Ca	
Na	
P	
K	
CIA.K	Chemical Index of Alteration minus Potassium
P_Sheldon	MAP (calculated as per Sheldon, 2002); ~8% 1σ propagated analytical uncertainty
Mr	Saturation isothermal remanent magnetization (typically magnetized in 1T; Am^2)
Ms	Saturation moment (Am^2)
Mr.Ms	Squareness ratio, Mr/Ms
Hc	Bulk Coercivity (T)
Hcr	Coercivity of remanence (T)
Hcr.Hc	Coercivity ratio, Hcr/Hc
Xi	Initial magnetic susceptibility (Am^2/T)
Xhf	High-field magnetic susceptibility (Am^2/T)

; (e.g. ARG10-001 or SGB09-117)

Table DR3. Testing hypotheses relating phytolith assemblage composition with different measurements of sediment transport.

Hypothesis	Metrics to be compared	Data	# samples	Data transformation	Test	p-value	Correlation coefficient
Relative abundance of palms in phytolith assemblages is correlated with relative abundance of fine sediment particles	PALM/(PALM+Other FI+GSSC) (%) vs. relative abundance of 5-15 micrometer sedimentary particles (%)	All samples with phytolith and grain size information (excluding fluvial facies)	16*	Square-root	Pearson's product-moment correlation	0.3065	0.2729
				None	Spearman rank correlation**	0.1229	0.4029
				None	Kendall's rank correlation**	0.0961	0.3167
				None	Gamma statistic	N/A	0.3167
Relative abundance of blackened palm phytoliths is correlated with relative abundance of fine sediment particles	BP (%) vs. relative abundance of 5-15 micrometer sedimentary particles (%)	All samples with phytolith and grain size information (excluding fluvial facies)	16*	Square-root	Pearson's product-moment correlation	0.5139	0.1762
				None	Spearman rank correlation	0.6968	0.1059
				None	Kendall's rank correlation	0.6901	0.0833
Phytolith yield is correlated with relative abundance of blackened palm phytoliths	Phytolith yield (mm3/g) vs. BP (%)	All samples with phytolith and grain size information (excluding fluvial facies)	22*	Square-root	Pearson's product-moment correlation	**0.0001**	**-0.7314**
				None	Spearman rank correlation**	**0.0014**	**-0.6380**
				None	Kendall's rank correlation**	**0.0017**	**-0.4891**
				None	Gamma statistic	N/A	-0.4978
		NSO sample subset	14	Square-root	Pearson's product-moment correlation	0.0573	-0.5007
				None	Spearman rank correlation**	0.1668	-0.3763
				None	Kendall's rank correlation**	0.2328	-0.2319
				None	Gamma statistic	N/A	-0.2353
		SO sample subset	7*	Square-root	Pearson's product-moment correlation	**0.0017**	**-0.9395**
				None	Spearman rank correlation**	**0.0028**	**-0.9643**
				None	Kendall's rank correlation**	**0.0028**	**-0.9048**
				None	Gamma statistic	N/A	-0.9048

BP = relative abundance of blackened palms, see Table DR1; NSO = samples with no indications of soil formation; SO = sampes from levels with clear indications of soil formation (root traces, burrows and other trace fossils, nodules); * = sample PB24838 excluded; ** = one or more ties present in data, resulting in inexact p-values. For other abbreviations, see Table DR1.